Applied Thermal Engineering 30 (2010) 1426–1437

Contents lists available at ScienceDirect

Applied Thermal Engineering

journal homepage: www.elsevier.com/locate/apthermeng

Numerical study of heat and mass transfer in the plate methanol steam micro-reformer channels

Ching-Yi Hsueh [a], Hsin-Sen Chu [a,b], Wei-Mon Yan [c,*], Chiun-Hsun Chen [a], Min-Hsing Chang [d]

[a] Department of Mechanical Engineering, National Chiao Tung University, Hsin-Chu 300, Taiwan, ROC
[b] Industrial Technology Research Institute, Chu-Tung, Hsin-Chu 310, Taiwan, ROC
[c] Department of Greenergy, National University of Tainan, Tainan 700, Taiwan, ROC
[d] Department of Mechanical Engineering, Tatung University, Taipei 104, Taiwan, ROC

ARTICLE INFO

Article history:
Received 12 August 2009
Accepted 2 March 2010
Available online 6 March 2010

Keywords:
Micro-reformer
Methanol
Heat and mass transfer
Numerical analysis

ABSTRACT

Effects of geometric and thermo-fluid parameters on performance and heat and mass transfer phenomena in micro-reformer channels were investigated by mathematical modeling. The geometric parameters considered were the channel length, channel height, catalyst thickness and catalyst porosity, while the thermo-fluid parameters included wall temperature, inlet fuel temperature, fuel ratio and Reynolds number. The results of the modeling suggest that the methanol conversion could be improved by 49%-points by increasing the wall temperature from 200 °C to 260 °C. The results also show that the CO concentration would be reduced from 1.72% to 0.95% with the H_2O/CH_3OH molar ratio values ranging from 1.0 to 1.6. The values of parameters that enhance the performance of micro-reformer were identified, such as longer channel length, smaller channel height, thicker catalyst layer, larger catalyst porosity, lower Reynolds number and higher wall temperature.

1. Introduction

In recent years, the proton exchange membrane fuel cell (PEMFC) and the direct methanol fuel cell (DMFC) have become widely used as miniature fuel cells [1]. While the PEMFC has high energy density, it needs to carry enough hydrogen fuel. Therefore, methanol steam micro-reformers are being developed for using with the miniature PEMFCs, to overcome the high risk of carrying a large quantity of hydrogen. Thus, there has been much interest in developing also methanol steam micro-reformers.

Several experiments for methanol steam reformers are currently in progress [2–9]. Various reformer types have been used as the foundation for methanol steam reformer designs, including packed-bed reformers and plate reformers. Several successfully fabricated packed-bed reformers for hydrogen production have been reported [2,3]. Kolb et al. [4] presented that the plate reformers have better performance than the packed-bed reformers due to better heat and mass transfers. Therefore, the channels were patterned on the plate methanol steam reformers by several investigators [5–9]. Their results showed that the plate methanol steam reformers were being developed to produce hydrogen for fuel cell systems.

Recently, many simulation studies have been made of the plate methanol steam reformer [10–21]. There have been various numerical studies of the fluid flow in plate methanol steam reformer channels [10,11]. Kwon et al. [10] investigated the pressure and velocity distributions in the micro-reformer channels by using computational fluid dynamics (CFD). The results show the reformer of 17 parallel micro-channels has a much more uniform velocity distribution than that of 36 parallel micro-channels. A uniform velocity distribution may have a better chemical reaction. A three-dimensional model of a micro-scale reactor to investigate velocity and pressure distributions was developed by Pattekar and Kothare [11]. In order to simplify the analysis, many studies have considered the numerical model of methanol steam reformers, only including energy equation and concentration equations with chemical reaction [12–14]. Kawamura et al. [12] proposed a mathematical heat and mass model to analyze the transport phenomena in the plane methanol steam reformer channels. Kim and Kwon [13] have numerically investigated the inner transport phenomena in the plate methanol steam reformer ducts. The results indicated that a lower inlet feed rate has a better methanol conversion. Varesano et al. [14] used a one-dimensional transient mathematical model to study the transport behaviors in a steam reforming reformer with a burner. Furthermore, the continuity equation, momentum equation, energy equation and species equations with chemical reaction were employed to explore the

* Corresponding author. Tel.: +886 6 260 2251; fax: +886 6 260 2205.
E-mail address: wmyan@mail.nutn.edu.tw (W.-M. Yan).

1359-4311/$ – see front matter © 2010 Elsevier Ltd. All rights reserved.
doi:10.1016/j.applthermaleng.2010.03.002

Nomenclature

C_i	concentration of species i (mol m^{-3})
c_p	specific heat at constant pressure (kJ kg^{-1} K^{-1})
D	hydraulic diameter (m)
D_{eff}	effective mass diffusivity (m^2 s^{-1})
D_k	mass diffusion coefficient (m^2 s^{-1})
D_p	catalyst particle diameter (m)
E_a	activation energy (kJ mol^{-1})
H	channel height (m)
ΔH_{SR}	enthalpy of reaction for steam reforming (kJ mol^{-1})
ΔH_{rWGS}	enthalpy of reaction for the reverse water–gas-shift (kJ mol^{-1})
k_{eff}	effective thermal conductivity(W m^{-1} K^{-1})
k_f	fluid phase thermal conductivity (W m^{-1} K^{-1})
k_p	permeability (m^2)
k_s	solid medium thermal conductivity (W m^{-1} K^{-1})
k_1	pre-exponential factor for steam reforming
k_2	pre-exponential factor for the reverse water–gas-shift
k_{-2}	pre-exponential factor for the water–gas-shift
L	channel length (m)
M_i	mole fraction of species i
$M_{w,i}$	molecular weight of species i (kg mol^{-1})
m_i	mass fraction of species i
p	pressure (Pa)
R	universal gas constant (kJ kg^{-1} K^{-1})
Re	Reynolds number, Re $= \rho u D/\mu$
R_{SR}	Arrhenius reaction rate coefficient for steam reforming (mol m^{-3} s^{-1})
R_{rWGS}	Arrhenius reaction rate coefficient for the reverse water–gas-shift reaction (mol m^{-3} s^{-1})
S_c	species source term for chemical reaction
S_u, S_v	momentum source terms for the porous medium in the x and y directions, respectively.
S_t	energy source term for chemical reaction
T	temperature (°C)
T_w	wall temperature (°C)
x, y	coordinates (m)
u, v	velocity components in the x and y directions, respectively (m s^{-1})

Greek symbols

β	inertial loss coefficient
γ	H_2O/CH_3OH molar ratio
δ_1	flow channel height (m)
δ_2	catalyst layer height (m)
ε	porosity
η	methanol conversion
λ_i'	the stoichiometric coefficient for reactant i in reaction
λ_i''	the stoichiometric coefficient for product i in reaction
τ	tortuosity of the porous medium
μ	dynamic viscosity (kg m^{-1} s^{-1})
μ_{mix}	viscosity of the gas mixture (kg m^{-1} s^{-1})
ϕ_{ij}	an auxiliary term in calculating viscosity of gas mixture
ρ	density (kg m^{-3})
ρ_s	catalyst density (kg m^{-3})

Subscripts

0	inlet

temperature and gas concentration distributions in the reformer by several researchers [15–21]. Park et al. [15] developed 3-D, quasi-3-D and 1D models to study reformer performance. There was good agreement between the experimental and analytical results. Hsueh et al. [16] employed a numerical channel model to analyze various height and width ratios on the plate micro-reformer performance and reactant gas transport characteristics. The results indicated that a reduction in aspect ratio would improve H_2 production rate and methanol conversion. Arzamendi et al. [17] established a micro channel model of the thermal integration of steam reformer and catalytic combustor. The results showed that the short diffusion distance and higher area to volume ratio were obtained by using the micro-reformers. A plate methanol reformer model was proposed by Pan and Wang [18]. Their numerical model accurately predicted the methanol conversion and the gas distributions. Kim and Kown [19] developed a novel reforming channel to study the pressure, velocity, temperature and hydrogen mole fraction distributions in the reformer. The results show that the novel flow field had better performance than the serpentine flow field. Kim [20] developed a micro-reformer model to simulate the conversion and temperature distributions in the reformer. The results revealed that the methanol conversion increased with increasing the reformer temperature and decreasing the feed rate. Chen et al. [21] used a mathematical model of the plate-type reformer to investigate the heat and mass transfer in a reformer. The results showed that the CO concentration could reduce with lower temperature, larger H_2O/CH_3OH molar ratio and aspect ratio. In this work, an attempt is made to examine the detailed fluid flow, heat and mass transfer coupled with chemical reactions in the plate methanol steam micro-reformer channels.

Although a channel model of the plate methanol steam reformer may be well established in the previous work [16], some of the geometric and thermo-fluid parameters aspects have not been addressed so far. Therefore, the effects of the geometric and thermo-fluid parameters on the plate methanol steam micro-reformer performance and the heat and mass transfer are numerically investigated in detail. In this work, a numerical model was developed to study the methanol conversion and local heat and mass transfer in the channel of a micro-reformer. The information reported here would be useful in improving plate methanol steam reformer performance.

2. Model description

Fig. 1 presents a schematic of the two-dimensional channel geometry of the plate methanol steam micro-reformer used in the present work. To simplify the analysis, the following assumptions are made:

(1) The flow is steady and laminar;
(2) The inlet fuel is an ideal gas;
(3) The flow is incompressible;
(4) The catalyst layer is an isotropic porous medium; and
(5) Thermal radiation and conduction in the gas phase are negligible compared to convection.

According to the model descriptions and assumptions above, the equations for a two-dimensional channel in the plate methanol reformer system are:

Continuity equation:

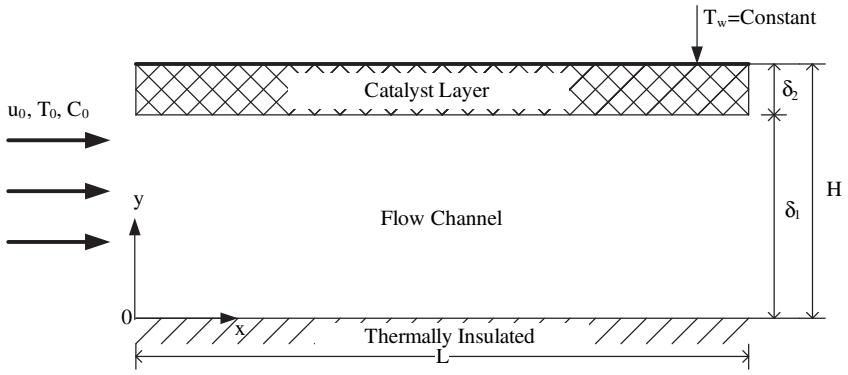

Fig. 1. Schematic diagram of the system.

$$\rho\left(\frac{\partial u}{\partial x}+\frac{\partial v}{\partial y}\right) = 0 \tag{1}$$

Momentum equation (x-coordinate):

$$\varepsilon\rho\left(u\frac{\partial u}{\partial x}+v\frac{\partial u}{\partial y}\right) = -\varepsilon\frac{\partial p}{\partial x}+\varepsilon\mu\left(\frac{\partial^2 u}{\partial x^2}+\frac{\partial^2 u}{\partial y^2}\right)+S_u \tag{2}$$

Momentum equation (y-coordinate):

$$\varepsilon\rho\left(u\frac{\partial v}{\partial x}+v\frac{\partial v}{\partial y}\right) = -\varepsilon\frac{\partial p}{\partial y}+\varepsilon\mu\left(\frac{\partial^2 v}{\partial x^2}+\frac{\partial^2 v}{\partial y^2}\right)+S_v \tag{3}$$

The S_u and S_v are zero in the flow channel region, and in the catalyst layer, they are as follows [22]:

$$S_u = -\frac{\mu u}{k_p}-\frac{\beta u\rho}{2}\sqrt{u^2+v^2} \tag{4}$$

$$S_v = -\frac{\mu v}{k_p}-\frac{\beta v\rho}{2}\sqrt{u^2+v^2} \tag{5}$$

where

$$k_p = \frac{D_p^2\varepsilon^3}{150(1-\varepsilon)^2} \tag{6}$$

$$\beta = \frac{3.5(1-\varepsilon)}{D_p\varepsilon^3} \tag{7}$$

The viscosity of the gas mixture can be calculated from Wilke's mixture rule [23] as follows:

$$\mu_{mix} = \sum_{i=1}^{5}\frac{M_i\mu_i}{\sum_{j=1}^{5}M_j\phi_{ij}} \tag{8}$$

where

$$\phi_{ij} = \sum_i \frac{\left[1+\left(\mu_i/\mu_j\right)^{1/2}\left(M_{w,j}/M_{w,i}\right)^{1/4}\right]^2}{\left[8\left(1+\left(M_{w,i}/M_{w,j}\right)\right)\right]^{1/2}} \tag{9}$$

Species equation:

$$\left(u\frac{\partial m_i}{\partial x}+v\frac{\partial m_i}{\partial y}\right) = D_{eff}\left(\frac{\partial^2 m_i}{\partial x^2}+\frac{\partial^2 m_i}{\partial y^2}\right)+(1-\varepsilon)\rho_s S_c \tag{10}$$

In the species equations, m_i denotes the mass fraction of the i-th species, including CH_3OH, H_2O, H_2, CO_2 and CO. The Stefan–Maxwell equations were used to calculate the mass diffusion coefficient [24]. The effective mass diffusivity D_{eff} is expressed as $D_{eff} = \varepsilon^{\tau}D_k$, where ε, the porosity of the medium, is expressed as 0.38 and 1.00, respectively, in the catalyst layer and the flow channel. There is no chemical reaction in the flow channel, so S_c is zero in the flow channel. In the catalyst layer where the chemical reaction takes place, the reaction model of Purnama et al. [25] is adopted to describe the source term.

$$S_c = M_{w,i}(R_{SR}+R_{rWGS})(\lambda_i''-\lambda_i') \tag{11}$$

Purnama et al. [25] and Agrell et al. [26] proposed that using a $Cu/ZnO/AlO_3$ catalyst for methanol steam reforming gives rise to two main chemical reactions, the steam reforming and the reverse water–gas-shift reactions. They also indicated that CO was generated by the reverse water–gas-shift reaction. Pan and Wang [18] and Purnama et al. [25] presented the following relations for the steam reforming reaction and the reverse water–gas-shift reaction:

$$CH_3OH + H_2O \xrightarrow{k_1} CO_2 + 3H_2 \tag{12}$$

$$CO_2 + H_2 \underset{k_{-2}}{\overset{k_2}{\leftrightarrow}} CO + H_2O \tag{13}$$

Table 1
Parameters used in this work.

Channel length L (m) [5]	3.3×10^{-2}
Channel height H (m) [5]	2.0×10^{-4}
Catalyst layer thickness δ_2 (m)	3.0×10^{-5}
Flow channel height δ_1 (m)	1.7×10^{-4}
Inlet average velocity u_0 (m s^{-1}) [5]	0.266
Inlet average temperature T_0 (°C) [5]	393
Operation pressure (atm) [5]	1
Activation energy for steam reforming (kJ mol^{-1}) [18]	76
Activation energy for reverse water–gas-shift (kJ mol^{-1}) [18]	108
Catalyst density (kg m^{-3}) [24]	1480
Catalyst thermal conductivity (W m^{-1} K^{-1}) [24]	0.3
Catalyst layer porosity [11]	0.38
Catalyst permeability (m^2) [11]	2.379×10^{-12}
Mass diffusion coefficient (m^2 s^{-1}) [24]	6.8×10^{-5}

Table 2
Methanol mole fractions for the various grids.

Gridlines	x (m)					
	0.005	0.010	0.015	0.020	0.025	0.030
71 × 16	0.377	0.309	0.261	0.224	0.194	0.171
91 × 26	0.378	0.309	0.261	0.224	0.194	0.171
111 × 41	0.378	0.309	0.261	0.224	0.194	0.173

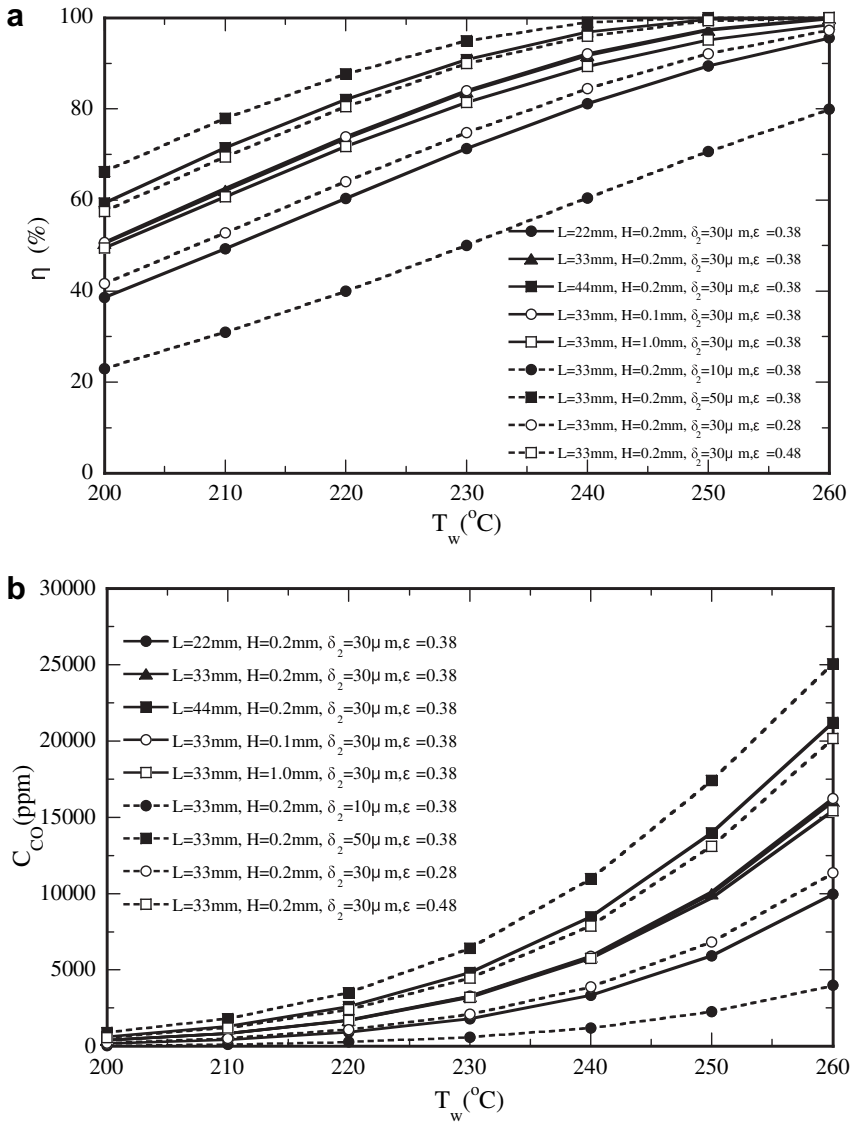

Fig. 2. Effects of geometric parameters and wall temperature on (a) the methanol conversion and (b) the CO concentration (ppm) at the outlet.

$$R_{SR} = k_1 C_{CH_3OH}^{0.6} C_{H_2O}^{0.4} \exp\left(-\frac{E_a}{RT}\right) \quad (14)$$

$$R_{rWGS} = k_2 C_{CO_2} C_{H_2} \exp\left(-\frac{E_a}{RT}\right) - k_{-2} C_{CO} C_{H_2O} \exp\left(-\frac{E_a}{RT}\right) \quad (15)$$

where the steam reforming reaction is a non-reversible reaction and the reverse water–gas-shift reaction is reversible.

Energy equation:

$$\rho c_p \left(u\frac{\partial T}{\partial x} + v\frac{\partial T}{\partial y}\right) = k_{eff}\left(\frac{\partial^2 T}{\partial x^2} + \frac{\partial^2 T}{\partial y^2}\right) + (1-\varepsilon)\rho_s S_t \quad (16)$$

In the energy equation, the effective thermal conductivity is:

$$k_{eff} = \varepsilon k_f + (1-\varepsilon)k_s \quad (17)$$

In the energy equation, S_t in the channel is zero. The catalyst layer experiences exothermic and endothermic chemical reactions, so S_t can be described as:

$$S_t = -(\Delta H_{SR} R_{SR} + \Delta H_{rWGS} R_{rWSG}) \quad (18)$$

The boundary conditions are given at the inlet, outlet, wall, and the interface between the channel and the catalyst layer for the numerical model. For the inlet condition ($x = 0$), the inlet boundary conditions are:

$$u = u_0 \quad (19)$$

$$m_i = m_{0,i} \quad (20)$$

$$T = T_0 \quad (21)$$

At the channel outlet ($x = L$), fully developed flow is assumed and the boundary conditions of velocity, temperature and mass fraction are expressed as:

$$\frac{\partial u}{\partial x} = v = 0, \quad \frac{\partial m_i}{\partial x} = 0, \quad \frac{\partial T}{\partial x} = 0 \quad (22)$$

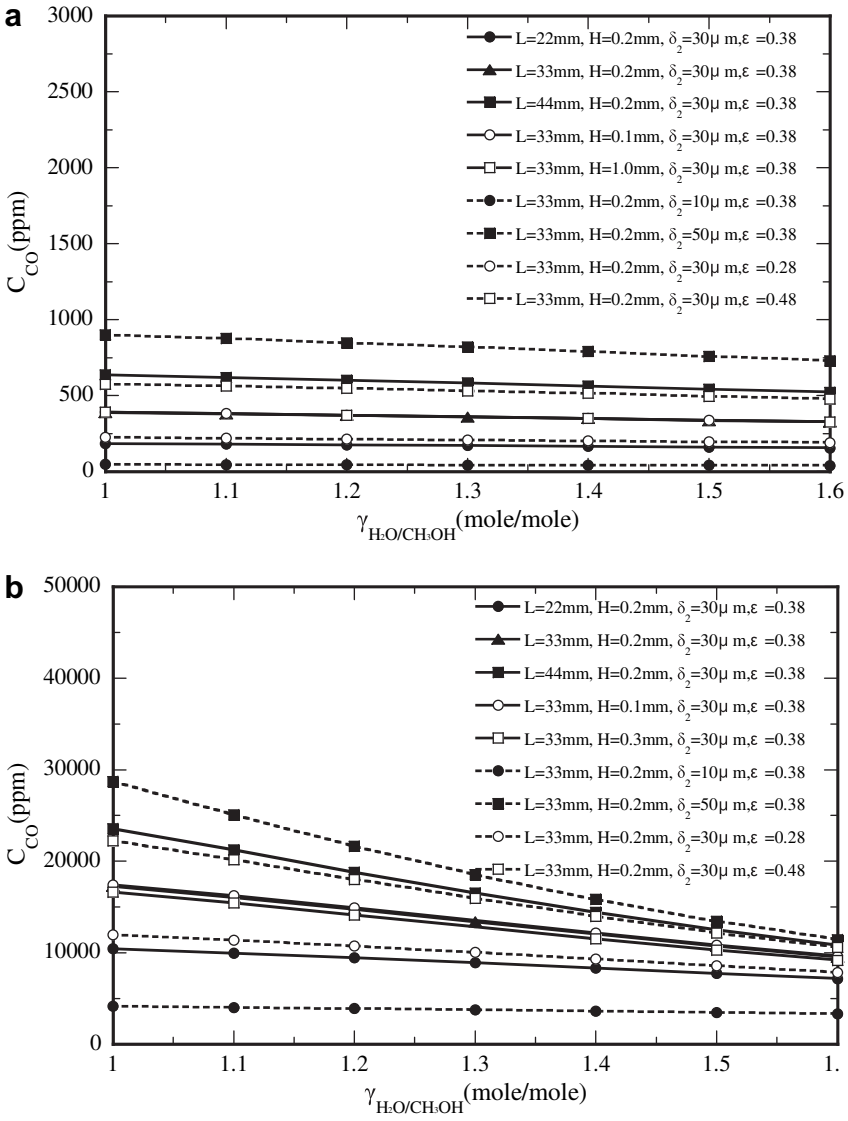

Fig. 3. Effects of geometric parameters and H_2O/CH_3OH molar ratio on the CO concentration at (a) $T_w = 200$ °C and (b) $T_w = 260$ °C.

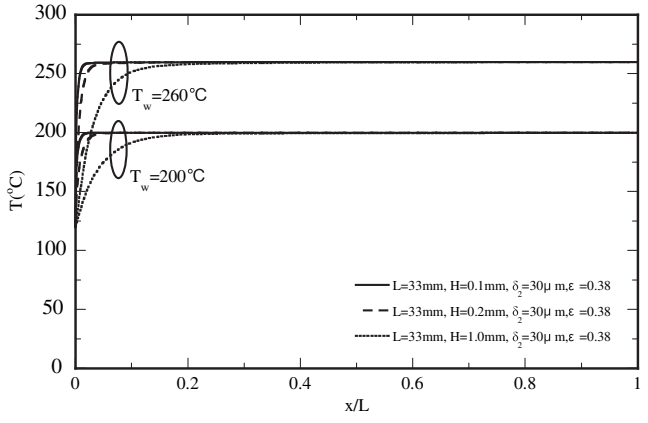

Fig. 4. Effects of the channel heights on temperature distributions along the centerline of the channel at $T_w = 200$ °C and $T_w = 260$ °C.

At the insulated plate ($y = 0$), the velocities and the temperature and mass fraction gradients are zero.

$$u = v = 0, \quad \frac{\partial m_i}{\partial y} = 0, \quad \frac{\partial T}{\partial y} = 0 \tag{23}$$

At the interface between the flow channel and the catalyst layer ($y = H - \delta_2$), the velocities and the temperature and mass fraction gradients are all continuous.

$$u_{y=(H-\delta_2)^+} = u_{y=(H-\delta_2)^-}, \quad \mu\frac{\partial u}{\partial y}\Big|_{y=(H-\delta_2)^+} = \mu\frac{\partial u}{\partial y}\Big|_{y=(H-\delta_2)^-} \tag{24}$$

$$C_{i,y=(H-\delta_2)^+} = C_{i,y=(H-\delta_2)^-}, \quad D_{\mathrm{eff},(H-\delta_2)^+}\frac{\partial m_i}{\partial y}\Big|_{y=(H-\delta_2)^+} = D_{\mathrm{eff},(H-\delta_2)^-}\frac{\partial m_i}{\partial y}\Big|_{y=(H-\delta_2)^-} \tag{25}$$

$$T_{y=(H-\delta_2)^+} = T_{y=(H-\delta_2)^-}, \quad k_{\mathrm{eff},(H-\delta_2)^+}\frac{\partial T}{\partial y}\Big|_{y=(H-\delta_2)^+} = k_{\mathrm{eff},y=(H-\delta_2)^-}\frac{\partial T}{\partial y}\Big|_{y=(H-\delta_2)^-} \tag{26}$$

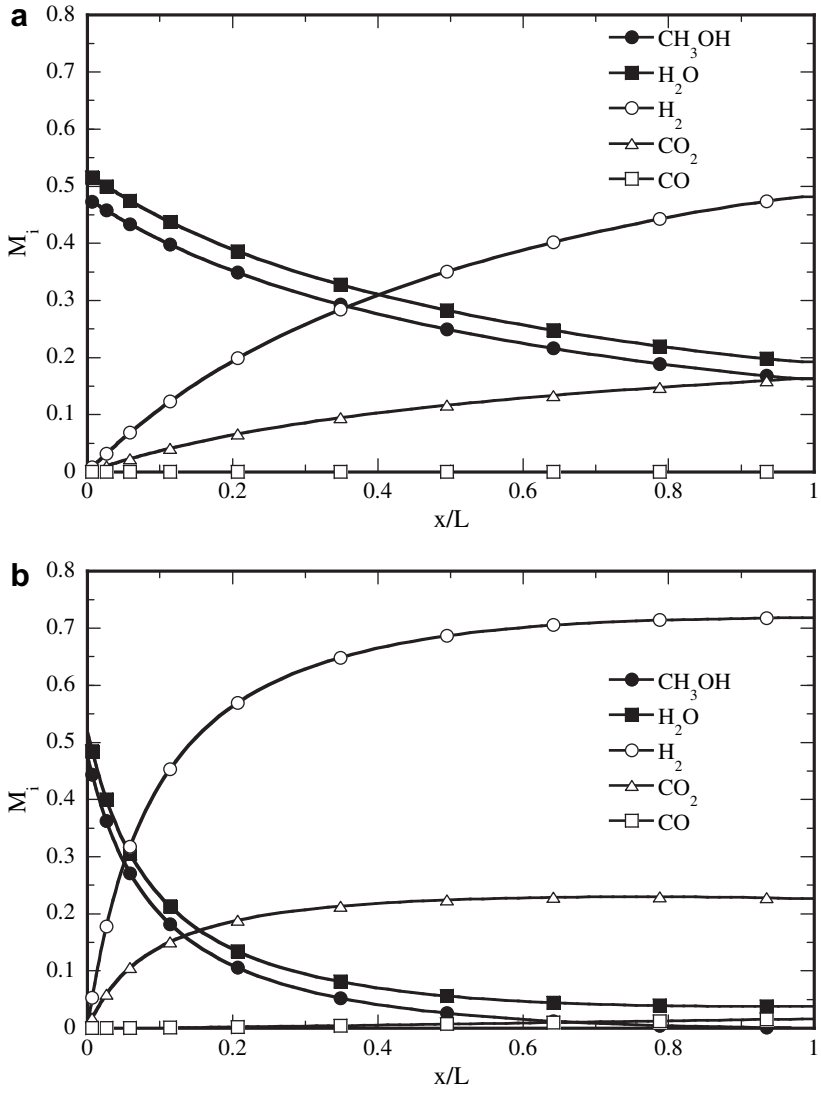

Fig. 5. Variations of the mole fraction of the various species along the channel at (a) $T_w = 200$ °C and (b) $T_w = 260$ °C.

At the heated wall ($y = H$), the velocities and the mass fraction gradient are zero, and the temperature is equal to the wall temperature:

$$u = v = 0, \quad \frac{\partial m_i}{\partial y} = 0, \quad T = T_w \tag{27}$$

3. Numerical method

A generalized form of the convection–diffusion transport equation was numerically solved using the commercial CFD program, FLUENT® 6.1. The finite difference method uses the control volume formulation with the SIMPLE algorithm to solve the mathematical model. The parameters used in the work are listed in Table 1. The convergence criterions for the normalized residuals for each variable were restricted to less than 10^{-6}. The effects of the number of gridlines on the numerical results are shown in Table 2 for three different grids. The predicted methanol mole fraction distributions show that the deviations of the methanol mole fraction among these three grids are 1%. Therefore, the 91 × 26 grid is used in this work. The accuracy of the numerical results was validated by comparing the predicted methanol conversion with experimental results of Park et al. [5], and the agreement was good. More details were given elsewhere [16].

4. Results and discussion

The influences of the geometric parameters and thermo-fluid parameters on the performance of micro-reformer are considered of great importance. To this end, the effects of the channel length ($L = 22$ mm, 33 mm, and 44 mm), channel height ($H = 0.1$ mm, 0.2 mm, and 1.0 mm), catalyst thickness ($\delta_2 = 10$ μm, 30 μm and 50 μm) and catalyst porosity ($\varepsilon = 0.28$, 0.38, and 0.48) on the methanol conversion and CO concentration in the micro-reformer were investigated. Additionally, the Reynolds number (Re = 2.2, 4.4 and 6.6), fuel ratio ($\gamma = 1.0$, 1.3 and 1.6) and inlet temperature ($T_0 = 100$ °C, 120 °C, and 140 °C) are the key thermo-fluid parameters in micro-reformer channels which would affect the micro-reformer performance.

In Fig. 2(a), the effects of geometric parameters on methanol conversion of micro-reformer channel are presented as follows:

(a) The results show that the methanol conversion increases with an increase in the wall temperature T_w for all geometric

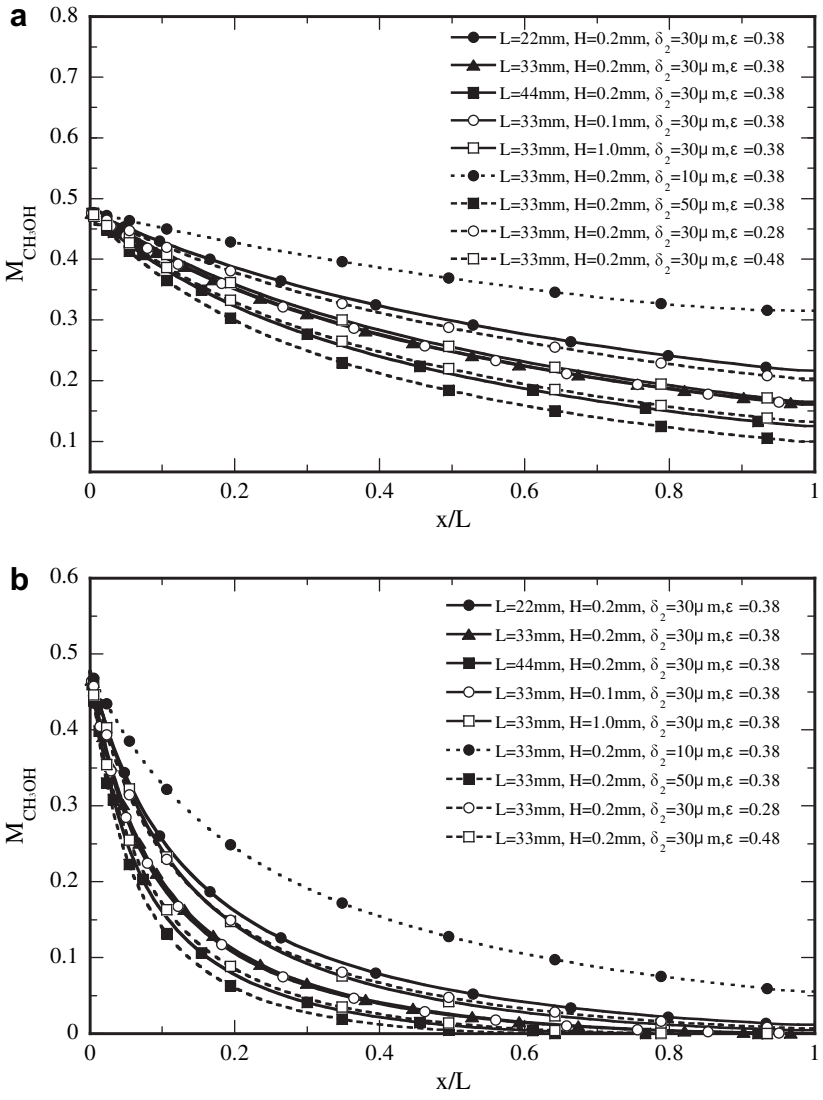

Fig. 6. Effects of geometric parameters on the local CH_3OH mole fraction along the channel at (a) $T_w = 200$ °C and (b) $T_w = 260$ °C.

conditions, implying that a better micro-reformer performance can be archived at higher wall temperature. By comparing the results of $T_w = 200$ °C and $T_w = 260$ °C with $L = 33$ mm, $H = 0.2$ mm, $\delta_2 = 30$ μm and $\varepsilon = 0.38$, it shows that the methanol conversion for $T_w = 260$ °C could be improved by 49%-points relative to that of $T_w = 200$ °C.

(b) Comparison of the corresponding curves of the channel lengths of $L = 22$ mm, 33 mm, and 44 mm indicates that better methanol conversion is found for a longer micro-reformer channel. This is due to the longer residence time of the fuel in the longer channel.

(c) As for the effects of channel heights ($H = 0.1$ mm, 0.2 mm, and 1.0 mm), the results reveal that all the three micro-channels possess a similar methanol conversion.

(d) It is seen in Fig. 2(a) that the methanol conversion in the micro-reformer is enhanced by the increased catalyst thickness. The channel with thicker catalyst layer has a larger chemical reaction area, which in turn causes a better methanol conversion. The results show that methanol conversion improves from 80% to 99% at $T_w = 260$ °C with the catalyst thickness ranging from 10 μm to 50 μm.

(e) The effects of the porosity of catalyst layer ($\varepsilon = 0.28$, 0.38, and 0.48) on methanol conversion of micro-reformer channel are also shown in Fig. 2(a). It is found that the methanol conversion increases with an increase in the porosity of catalyst layer. This means that reaction surface is enlarged via an increase in the catalyst porosity.

The best methanol conversion is noted for the case with $L = 33$ mm, $H = 0.2$ mm, $\delta_2 = 50$ μm and $\varepsilon = 0.38$ at $T_w = 260$ °C. This implies that the appropriate channel geometry and catalyst thickness are very critical for improving methanol conversion.

The CO concentration must be reduced for further use in a PEM fuel cell. Therefore, the CO concentration distributions for various geometric parameters are presented in Fig. 2(b). It is clearly observed that the CO concentration increases with increasing wall temperature. This is because the endothermic reverse water–gas-shift reaction increases as the wall temperature increases. It is clear in Fig. 2(b) that lower CO concentration is found for a micro-reformer with a shorter channel length. A detailed comparison of the corresponding curves shows that lower CO concentration is noted for a micro-reformer with a thinner catalyst thickness or

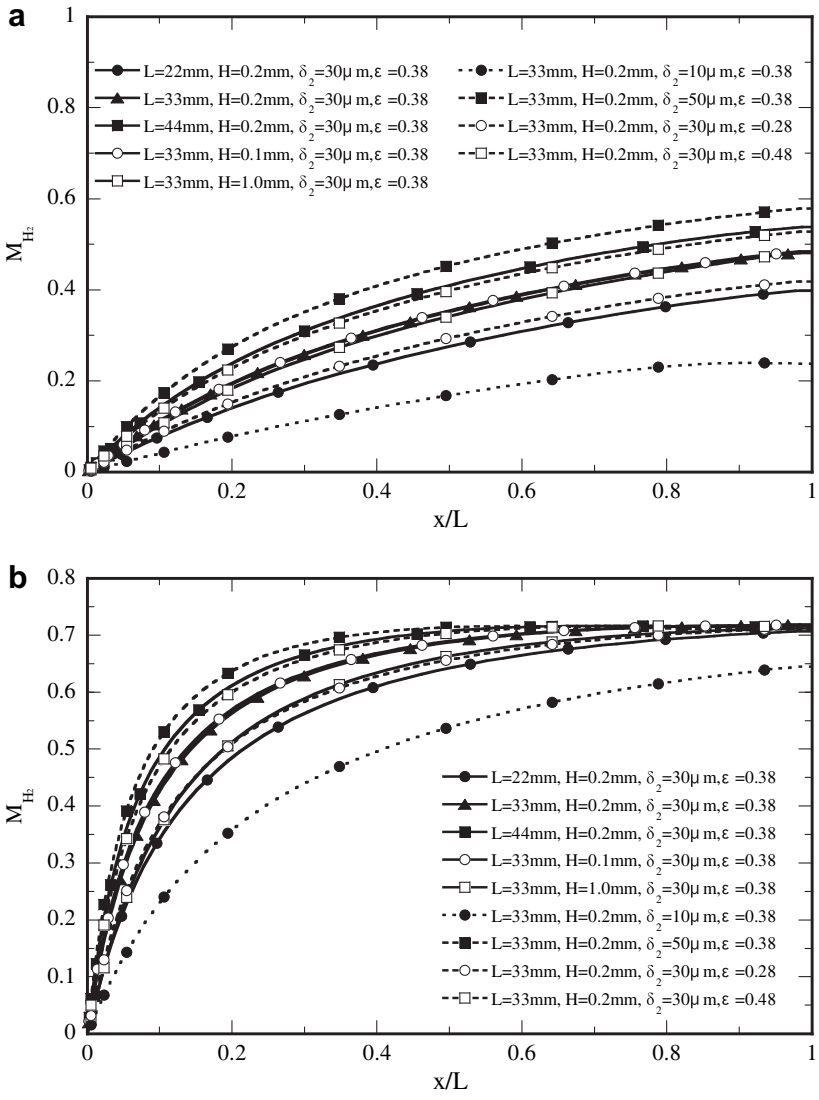

Fig. 7. Effects of geometric parameters on the local H_2 mole fraction along the channel at (a) $T_w = 200$ °C and (b) $T_w = 260$ °C.

a lower porosity. It is clearly seen that the CO concentration is about 16,000 ppm for the case with $L = 33$ mm, $H = 0.2$ mm, $\delta_2 = 30$ μm, $\varepsilon = 0.38$ and a wall temperature of 260 °C.

The effects of inlet fuel ratio on the CO concentration (ppm) at the outlet were also investigated. The effects of the molar ratio of H_2O/CH_3OH on the CO concentration for various geometric parameters and wall temperatures are shown in Fig. 3. A careful inspection of Fig. 3 discloses that the CO concentration decreases with an increase in the inlet molar ratio of H_2O/CH_3OH. This is due to the fact that the higher H_2O concentration enhances the water–gas-shift reaction which, in turn, reduces the CO concentration. The results also show that the CO concentration would be reduced from 1.72% to 0.95% at $T_w = 260$ °C with the H_2O/CH_3OH molar ratio values ranging from 1.0 to 1.6. However, the higher molar ratio of H_2O/CH_3OH also reduces the H_2 concentration at the channel outlet. It is also found that the effects of the H_2O/CH_3OH molar ratio on the CO concentration are more significant for a case with a higher wall temperature.

The impact of channel height on temperature distribution along the centerline of the channel, at a fixed Reynolds number, was examined for the heights 0.1 mm, 0.2 mm and 1 cm. The hydraulic diameters of channel vary depending on channel heights. A higher channel height has a greater hydraulic diameter. Fig. 4 illustrates that the centerline temperature increases along the channel as a consequence of the heated wall. For a smaller channel height, the temperature distribution is much more uniform due to the shorter thermal entrance length. This kind of uniform temperature distribution improves the chemical reaction rate. Therefore, as shown in Fig. 2, the methanol conversion of the micro-reformer is slightly enhanced with the smaller channel height at higher wall temperature. A comparison of the temperature distributions for wall temperatures of 200 °C and 260 °C indicates that the centerline temperature increases with an increase in the wall temperature.

Fig. 5 shows the local distributions of the different species at wall temperatures of 200 °C and 260 °C along the centerline of the channel for the same operating conditions. Fig. 5 discloses that both the mole fractions of the CH_3OH and H_2O decrease as the fluid moves downstream, while the H_2, CO_2 and CO mole fractions increase with axial location. Fig. 5 clearly demonstrates that the mole fractions of the products increase with an increase in the wall temperature. In addition, Fig. 5(b) shows that the methanol

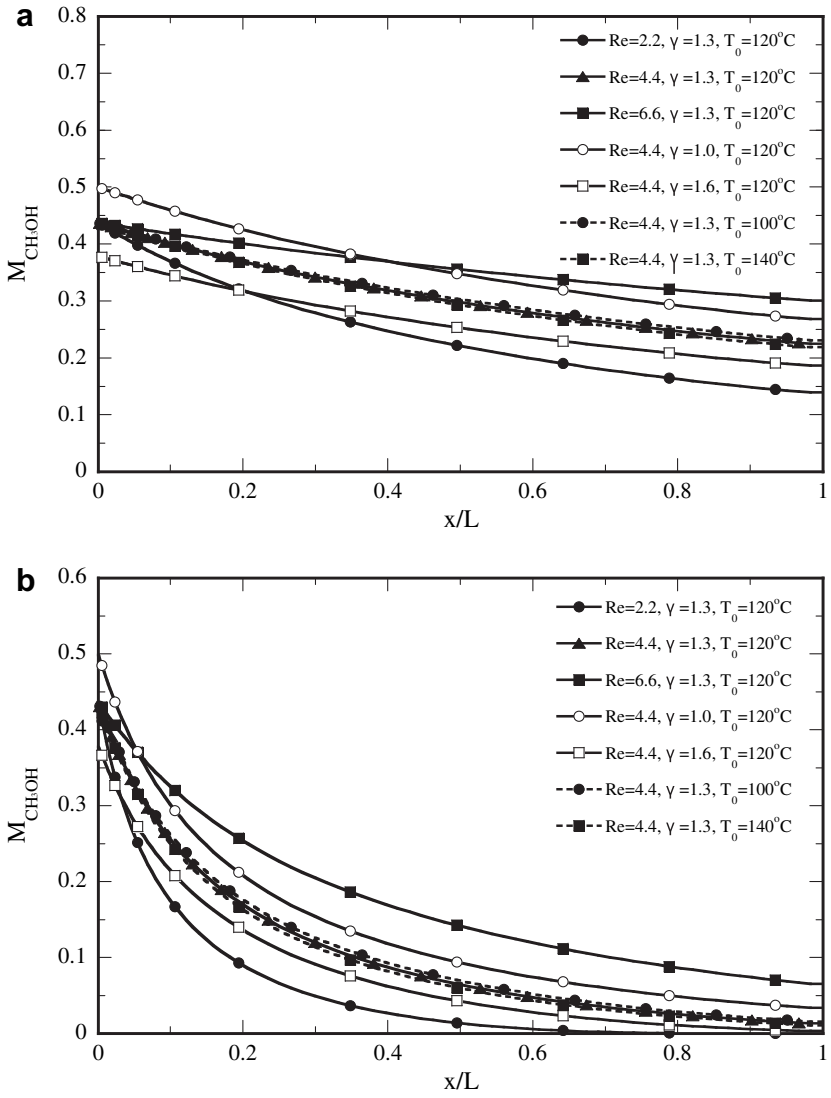

Fig. 8. Effects of thermo-fluid parameters on the local CH_3OH mole fraction along the channel at (a) $T_w = 200$ °C and (b) $T_w = 260$ °C.

conversion is greater than 99% at a wall temperature of 260 °C, with a product gas composition of 74.7% H_2, 23.6% CO_2 and 1.7% CO at the outlet of the channel. The results agree reasonably with experimental data [5]. For the PEM fuel cell, the CO concentration should be less than 10 ppm, so cleanup step is required after reforming. The utilization of the PrOx or water–gas-shift reaction equipment can reduce the CO concentration in the gas from the micro-reformer.

Studies of the reactant gas transport in micro-reformer channels have shown that a detailed understanding of the local distribution of the CH_3OH mole fraction along the channel is important for designing the micro-reformer. Therefore, the effects of geometric parameters on the local distributions of the CH_3OH mole fraction along the channel centerline are presented in Fig. 6. The results reveal that geometric parameters have a considerable impact on the local CH_3OH distributions. It is found that the CH_3OH mole fractions decrease as the fluid moves downstream due to the chemical reaction. For various channel heights, there appears to be little variation in the CH_3OH mole fraction distributions. The higher methanol concentration is noted for a system with a longer channel length or with a lower catalyst layer thickness and porosity. This implies that the chemical reaction rate is weaker for a system with a shorter channel length or with a lower catalyst layer thickness and porosity. The effect of wall temperature on the local CH_3OH mole fraction can be found by comparing the corresponding curves in Fig. 6(a) and (b). It is clear that smaller methanol concentration is noted for a case with a higher wall temperature. This can be explained by the fact that a stronger chemical reaction is experienced for a micro-reformer channel with a higher wall temperature.

The distributions of the H_2 mole fraction along the channel are shown in Fig. 7 for various geometric parameters and wall temperatures. A higher H_2 mole fraction along the channel represents a higher methanol conversion. Thus, the variation of the H_2 fraction is opposite to that of the CH_3OH mole fraction in Fig. 6. In Fig. 7, a higher H_2 mole fraction is found for a micro-reformer channel with a longer channel length or with a higher catalyst thickness, porosity and wall temperature.

The Reynolds number increases with increasing fuel velocities at the same inlet area. Fig. 8 shows the effects of the Reynolds number on the local distributions of the CH_3OH mole fraction along the channel at the same catalyst layer thickness and

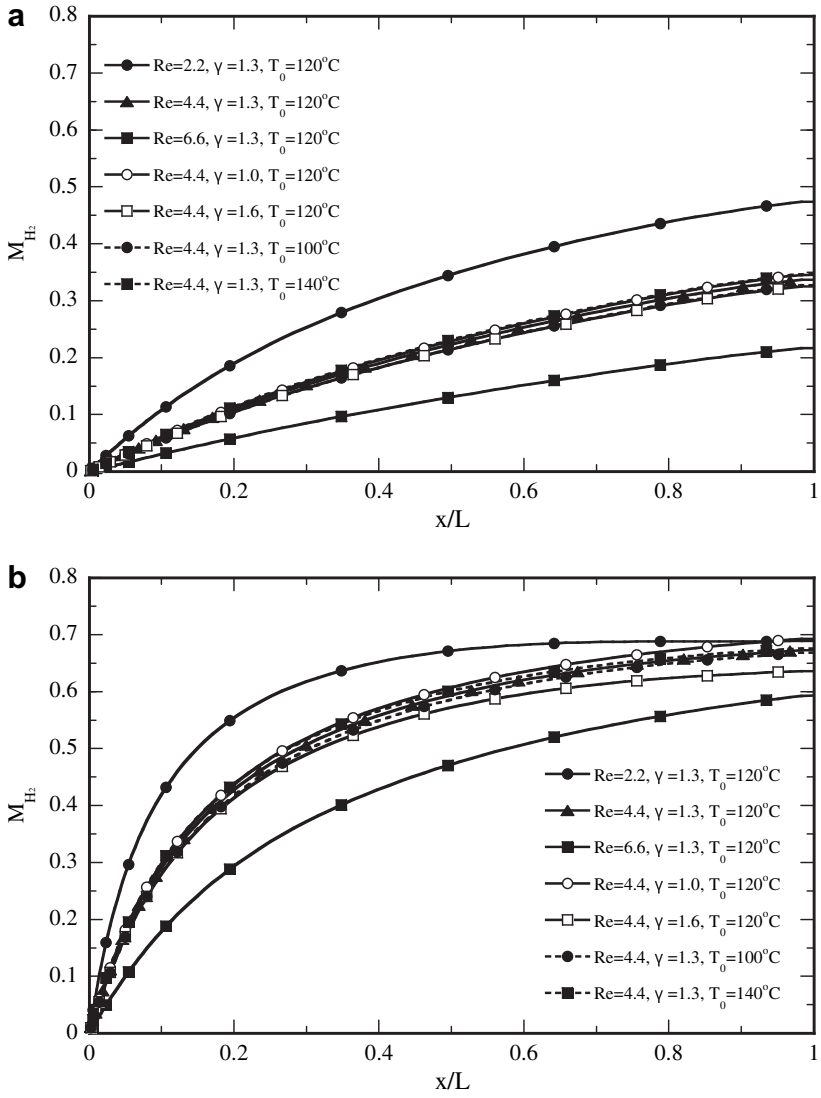

Fig. 9. Effects of thermo-fluid parameters on the local H_2 mole fraction along the channel at (a) T_w = 200 °C and (b) T_w = 260 °C.

porosity. Three cases with Reynolds number of 2.2, 4.4 and 6.6 are presented in Fig. 8. It is clearly observed a lower methanol concentration (better methanol conversion) is found for a micro-reformer channel with a lower Reynolds number. This is due to the fact micro-reformer channel with a lower Reynolds number would experience a longer reactant gas resident time and reaction time, which in turn causes a better methanol conversion. In this work, we considered the H_2O/CH_3OH molar ratio values 1.0, 1.3 and 1.6. The predicted results in Fig. 8 show that the CH_3OH concentration decreases with an increase in the H_2O/CH_3OH molar ratio. Also, the impact of different inlet fuel temperatures was examined for the values of 100 °C, 120 °C and 140 °C. It is found that a lower CH_3OH concentration (a better methanol conversion) is found for a system with a higher inlet fuel temperature which increases the reaction rate. Comparison of the local CH_3OH mole fractions in Fig. 8(a) and (b) for the wall temperatures of 200 °C and 260 °C for the various operating parameters shows that the local CH_3OH mole fraction decreases with increasing wall temperature due to a strong chemical reaction for a high wall temperature.

The dependence of the local H_2 mole fraction distribution on the Reynolds number, fuel ratio and inlet temperature are presented in Fig. 9. The results show that a higher H_2 mole fraction is noted for a micro-reformer channel with a lower Reynolds number. This is due to the longer gas resident time which results in a better methanol conversion and a higher H_2 production. The influences of the H_2O/CH_3OH molar ratio on the H_2 mole fraction are presented in Fig. 9. The results show that a higher molar ratio of H_2O/CH_3OH causes the H_2 mole fraction to fall. Additionally, the H_2 mole fraction increases with increasing inlet fuel temperature. Comparison of Fig. 9(a) and (b) indicates that a higher local H_2 mole fraction is experienced for a micro-reformer channel with a higher wall temperature owing to a stronger chemical reaction.

Fig. 10 presents the variations of the CO mole fractions along the channel for the various thermo-fluid parameters. By comparing Figs. 9 and 10, it is found that the CO distributions in Fig. 10 have the same trends as the H_2 distributions in Fig. 9. This confirms the common concept that a micro-reformer with a H_2 production indicates a higher CO concentration.

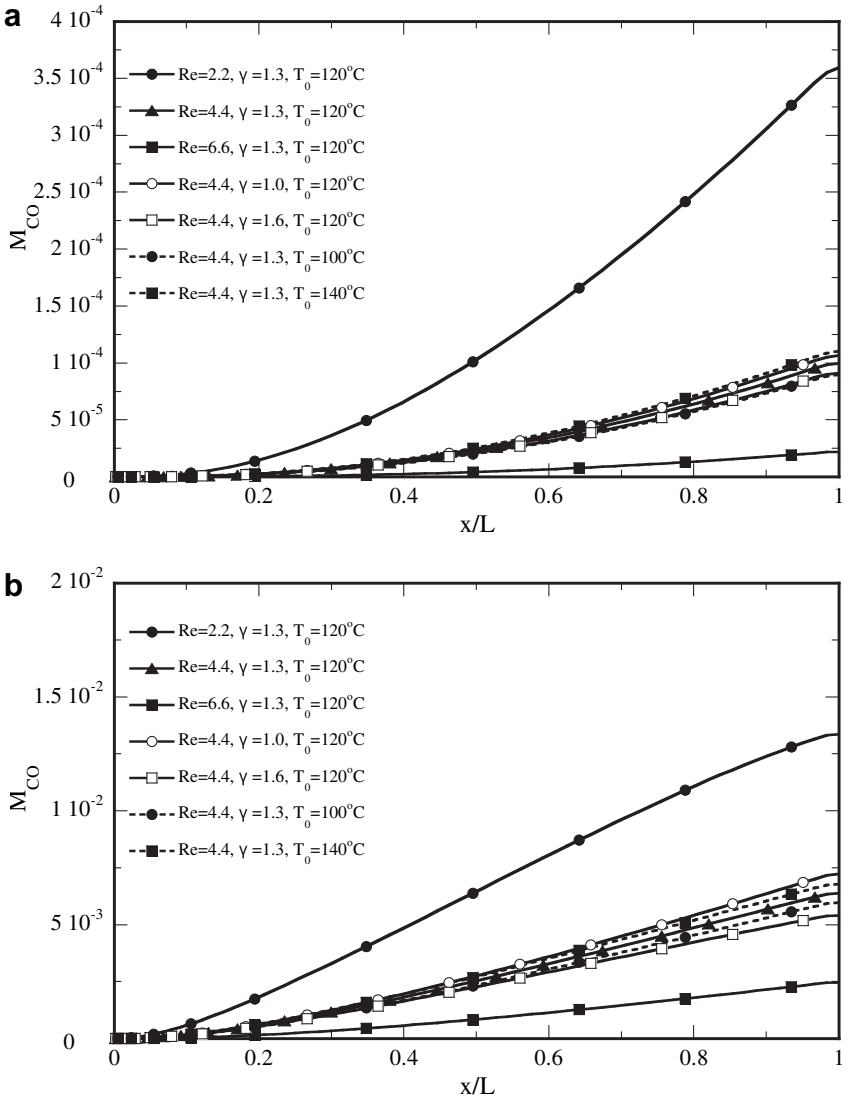

Fig. 10. Effects of thermo-fluid parameters on the local CO mole fraction along the channel at (a) $T_w = 200$ °C and (b) $T_w = 260$ °C.

5. Conclusions

This study numerically investigated the effects of the geometric and thermo-fluid parameters on the heat and mass transfer and methanol conversion in a micro-reformer channel. The conclusions drawn from the analyses are:

1. The effects of channel geometry and catalyst thickness have a significant impact on the methanol conversion and heat and mass transfer in the plate micro-reformer.
2. The micro-reformer performance increases with increasing wall temperature due to increase in the chemical reaction rate.
3. Smaller channel heights have much more uniform temperature distributions. Therefore, the methanol conversion of the micro-reformer is slightly enhanced with the smaller channel height at higher wall temperature.
4. A reduced Reynolds number for the reactant gas in the channel would rise the reactant gas residence time, which in turn, increases the reaction time and improves the methanol conversion.
5. The CO concentration decreases with increasing H_2O/CH_3OH molar ratio of the inlet fuel.

Acknowledgement

This study was supported by the National Science Council through grant number NSC 96-2212-E-211-004.

References

[1] A. Kundu, J.H. Jang, J.H. Gil, C.R. Jung, H.R. Lee, S.H. Kim, B. Ku, Y.S. Oh, Micro-fuel cells—current development and applications. J. Power Sources 170 (2007) 67–78.
[2] J.D. Holladay, E.O. Jones, R.A. Dagle, G.G. Xia, C. Cao, Y. Wang, High efficiency and low carbon monoxide micro-scale methanol processors. J. Power Sources 131 (2004) 69–72.
[3] M.T. Lee, R. Greif, C.P. Grigoropoulos, H.G. Park, F.K. Hsu, Transport in packed-bed and wall-coated steam-methanol reformer. J. Power Sources 166 (2007) 194–201.
[4] G. Kolb, V. Hessel, V. Cominos, C. Hofmann, H. Lowe, G. Nikolaidis, R. Zapf, A. Ziogas, E.R. Delsman, M.H.J.M. De Croon, J.C. Schouten, O. De La Iglesia, R. Mallada, J. Santamaria, Selective oxidations in micro-structured catalytic reactors – for gas-phase reactions and specifically for fuel processing for fuel cells. Catal. Today 20 (2007) 2–20.
[5] G.G. Park, D.J. Seo, S.H. Park, Y.G. Yoon, C.S. Kim, W.L. Yoon, Development of microchannel methanol steam reformer. Chem. Eng. J. 101 (2004) 87–92.
[6] D.E. Park, T. Kim, S. Kwon, C.K. Kim, E. Yoon, Micromachined methanol steam reforming system as a hydrogen supplier for portable proton exchange membrane fuel cells. Sens. Actuators A 135 (2007) 58–66.

[7] J.Y. Won, H.K. Jun, M.K. Jeon, S.I. Woo, Performance of microchannel reactor combined with combustor for methanol steam reforming. Catal. Today 111 (2006) 158–163.
[8] O.J. Kwon, S.M. Hwang, J.H. Chae, M.S. Kang, J.J. Kim, Performance of a miniaturized silicon reformer–PrOx-fuel cell system. J. Power Sources 165 (2007) 342–346.
[9] T. Kim, S. Kwon, MEMS fuel cell system integrated with a methanol reformer for a portable power source. Sens. Actuators A 162 (2009) 204–211.
[10] O.J. Kwon, D.H. Yoon, J.J. Kim, Silicon-based miniaturized reformer with methanol catalytic burner. Chem. Eng. J. 140 (2008) 466–472.
[11] A.V. Pattekar, M.V. Kothare, A microreactor for hydrogen production in micro fuel cell applications. J. Microelectromech. Syst. 13 (2004) 7–18.
[12] Y. Kawamura, N. Ogura, T. Yamamoto, A. Igarashi, A miniaturized methanol reformer with Si-based microreactor for a small PEMFC. Chem. Eng. Sci. 61 (2006) 1092–1101.
[13] T. Kim, S. Kwon, Design, fabrication and testing of a catalytic microreactor for hydrogen production. J. Micromech. Microeng. 16 (2006) 1760–1768.
[14] A. Varesano, I. Guaglio, G. Saracco, P.L. Maffettone, Dynamics of a methanol reformer for automotive applications. Ind. Eng. Chem. Res. 44 (2005) 759–768.
[15] H.G. Park, J.A. Malen, W.T. Piggott III, J.D. Morse, R. Greif, C.P. Grigoropoulos, Methanol steam reformer on a silicon wafer. J. Microelectromech. Syst. 15 (2006) 976–985.
[16] C.Y. Hsueh, H.S. Chu, W.M. Yan, Numerical study on micro-reformer performance and local transport phenomena of the plate methanol steam microreformer. J. Power Sources 187 (2009) 535–543.
[17] G. Arzamendi, P.M. Dieguez, M. Montes, M.A. Centeno, J.A. Odriozola, L. M. Gandia, Integration of methanol steam reforming and combustion in a microchannel reactor for H_2 production: a CFD simulation study. Catal. Today 143 (2008) 25–31.
[18] L. Pan, S. Wang, Modeling of a compact plate-fin reformer for methanol steam reforming in fuel cell systems. Chem. Eng. J. 108 (2005) 51–58.
[19] T. Kim, S. Kwon, MEMS fuel cell system integrated with a methanol reformer for a portable power source. Sens. Actuators A 154 (2009) 204–211.
[20] T. Kim, Micro methanol reformer combined with a catalytic combustor for a PEM fuel cell. Int. J. Hydrogen Energy 34 (2009) 6790–6798.
[21] F. Chen, M.H. Chang, C.Y. Kuo, C.Y. Hsueh, W.M. Yan, Analysis of a plate-type microreformer for methanol steam reforming reaction. Energy Fuels 23 (2009) 5092–5098.
[22] S. Ergun, Fluid flow through packed columns. Chem. Eng. Prog. 48 (1952) 89–94.
[23] F.M. White, Viscous Fluid Flow, second ed. McGraw-Hill, 1991.
[24] A. Karim, J. Bravo, D. Gorm, T. Conant, A. Datye, Comparison of wall-coated and packed-bed reactors for steam reforming of methanol. Catal. Today 110 (2005) 86–91.
[25] H. Purnama, T. Ressler, R.E. Jentoft, H. Soerijanto, R. Schlogl, R. Schomacker, CO formation/selectivity for steam reforming of methanol with a commercial $CuO/ZnO/Al_2O_3$ catalyst. Appl. Catal. A 259 (2004) 89–94.
[26] J. Agrell, H. Birgersson, M. Boutonnet, Steam reforming of methanol over a $Cu/ZnO/Al_2O_3$ catalyst: a kinetic analysis and strategies for suppression of CO formation. J. Power Sources 106 (2002) 249–257.